Available online at www.sciencedirect.com
ScienceDirect
Polymer 48 (2007) 6948–6954
polymer
www.elsevier.com/locate/polymer

Structure–property relationships in nanocomposites

Yves Termonia

Central Research and Development, Building E304, Room C219, Experimental Station, E.I. DuPont de Nemours, Inc., Wilmington, DE 19880-0304, United States

Received 21 August 2007; received in revised form 17 September 2007; accepted 18 September 2007
Available online 22 September 2007

Abstract

A numerical finite-difference model is presented for the study of the factors controlling the properties of composites reinforced with platelets and fiber-like nano-inclusions. The approach provides a comprehensive treatment of the dependence of composite modulus and strength on the shape of the inclusions and the interrelated effects of their orientation, volume fraction, aspect ratio, modulus and interfacial properties with the matrix. At the same volume fraction, we find that platelets are generally more efficient than fibers in improving composite modulus. This is rationalized through our model finding that fibers have a typically low critical aspect ratio value, which puts an upper limit to their reinforcement potential. Platelets also turn out to be superior to fibers in all nanocomposites characterized by a poor orientation of the inclusions. We also find that low interfacial adhesion and poor dispersion of the inclusions lead to a decrease in reinforcement efficiency. Turning to comparison with experiment, a good agreement is found between our model predictions and modulus data on nanocomposites reinforced with montmorillonite platelets and carbon nanotubes.

Keywords: Modeling; Composite; Nano-inclusions

1. Introduction

Recently, there has been a great interest in the use of nanoparticles for the reinforcement of polymeric materials. Typical inclusions are made of carbon nanotubes or clay platelets such as montmorillonite (MMT). Both structures are characterized by a very high modulus and aspect ratio and they offer exceptional reinforcement at low filler concentrations, often a fraction of what is typically required in conventional composites. In spite of its importance, there is still very little understanding of the dependence of nanocomposite properties on the intrinsic characteristics of the inclusions. These characteristics include aspect ratio, modulus, orientation and quality of the dispersion within the polymeric material.

Several analytical techniques have been introduced to answer these issues. Hui et al. [1,2] have studied the effect of modulus and aspect ratio of a single inclusion using simple engineering approximations based on the shear-lag model. Several authors [3–5] have extended the Halpin–Tsai equations and the Mori–Tanaka average stress theory to address the importance of orientation and partial exfoliation of clay platelets. Constitutive models have also been introduced for describing the stiffness of composites reinforced with carbon nanotubes [6].

Since these analytical approaches are limited to simple geometries, numerical simulation models have also been proposed. Buxton and Balazs [7] have introduced a three-dimensional lattice spring model to study the stress distribution around a single platelet. The deformation behavior of polymeric chains around nano-inclusions of various shapes has been investigated using rotational isomeric state models [8] which clearly indicate greater reinforcement from oblate particles. Molecular dynamics simulations [9,10] were later employed to calculate the stress–strain behavior of a polymer composite reinforced with single carbon nanotubes of two different lengths. Finite-element models have also been used by several researchers. Hine et al. [11] have studied the effects of aspect ratio and fiber length distribution. The study however

E-mail address: yves.termonia@usa.dupont.com

0032-3861/$ - see front matter © 2007 Elsevier Ltd. All rights reserved.
doi:10.1016/j.polymer.2007.09.025

was limited to small aspect ratio values not exceeding 50. The effect of fiber waviness was investigated by Fisher et al. [12]. Miyagawa et al. [13] applied the finite-element method to nanoclay inclusions but the investigation was again limited to small aspect ratios of 30, *vs*. several hundreds for actual clay platelets.

In a previous series of articles [14–16], we introduced a stochastic Monte–Carlo approach for the study of the tensile modulus and strength of short-fiber-reinforced composites. The approach is especially well suited for the study of tensile strength since it explicitly takes into account local stress concentrations at the interface between matrix and inclusion. In the model, the composite material is represented by a 3-dimensional lattice of bonds having different elastic constants for the inclusion and for the matrix. For a given value of external strain, the lattice sites are relaxed towards mechanical equilibrium with their neighbors by a systematic sequence of operations which steadily reduce the net residual force acting on each site. As the bonds are stretched, their local stresses combined with thermal activation rate theory [17] defining probabilities for bond rupture. Bonds belonging to the inclusion and to the matrix are allowed to break during the fracture of the composite. In the present work, this model is extended to the case of platelets and fiber inclusions of very high modulus and aspect ratio values, typical of those found in nanocomposite materials. The approach provides a comprehensive treatment of the dependence of composite mechanical properties on the interrelated effects of orientation, volume fraction, aspect ratio and modulus of the inclusions. Since the latter typically offer very large surface areas in all nanocomposite systems, our model also allows one to study in detail the importance of the thickness and modulus of the interfacial region between matrix and filler. Being on a mesoscopic scale, our approach however is incapable of predicting the properties of that interface for a given choice of inclusion and matrix. Complicating effects such as filler-induced crystallization deep inside the matrix are also beyond the scope of this work [18].

2. Model

Following Ref. [16], our model representation proceeds as follows. We start with a 3-dimensional x–y–z lattice of up to $300 \times 300 \times 300$ sites and choose the y direction as the tensile axis. The thickness of a platelet as well as the diameter of a fiber are set equal to one lattice unit so that the unit lattice length is of the order of 1 nm. For each inclusion to be constructed on the lattice, an orientation angle θ with respect to the y-axis is first selected according to the probability distribution

$$P(\theta) = \lambda^3 \left(\cos^2\theta + \lambda^3 \sin^2\theta\right)^{-3/2} \tag{1}$$

which leads to an average [16]

$$\left\langle \cos^2\theta \right\rangle = \left[\lambda^3/\left(\lambda^3-1\right)\right]\left\{1 - \left(\lambda^3-1\right)^{-1/2} \tan^{-1}\left[\left(\lambda^3-1\right)^{1/2}\right]\right\} \tag{2}$$

Eqs. (1) and (2) were originally introduced by Kuhn and Grun [19] to describe the orientation of chain vectors in an isotropic polymer following tensile deformation through a draw ratio λ. Henceforth, λ will be left as a free parameter used to control the distribution of orientations for an inclusion. These inclusions are constructed as follows. Starting from a site selected at random, a cluster of bonds is generated on the lattice by connecting the nearest neighbor sites along a direction at an angle θ with the y-axis. Upon reaching a preset aspect ratio value, a second cluster is started from another site and along a different θ value, again selected from Eq. (1) and so on and so forth until a predetermined fraction of bonds V_i for the inclusions is reached. Upon completion of that process, bonds along the tensile y-axis that belong to the inclusions are given an elastic constant E_i, whereas those in the transverse x- and z-axes are assigned a shear modulus value, G_i. Similarly, matrix bonds are given the modulus values E_m and G_m, depending on their orientation. Our model representation is schematically illustrated in Fig. 1 for the case of fiber inclusions randomly oriented in the x–y plane.

The lattice described above is strained in tension along the y-axis at a constant rate of deformation and temperature T. In the course of that process, bonds are broken according to the kinetic theory of fracture [20], *i.e*. at a rate

$$\nu = \tau \exp[(-U + \beta\sigma)/kT] \tag{3}$$

where U is the activation energy, τ is the thermal vibration frequency ($\sim 10^{12}$ s^{-1}) and β is the activation volume. In Eq. (3), σ is the local stress

$$\sigma = K\varepsilon \tag{4}$$

where K is the elastic constant for the bond whereas ε is the local strain. This bond-breaking process is executed with the help of a Monte–Carlo process (for more details, see Refs. [14,15]) which, at regular time intervals, also relaxes the lattice to its minimum energy configuration. That minimum is

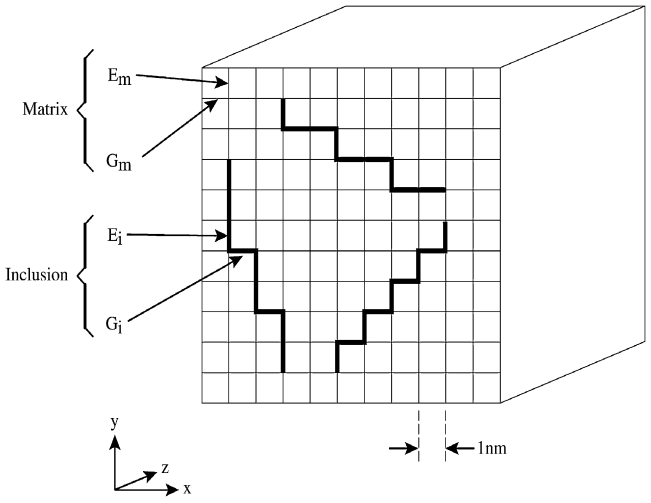

Fig. 1. Model representation of fiber inclusions randomly oriented in the x–y plane. The fiber aspect ratio is set at $l/d = 9$.

assumed to be reached when the net residual force on a lattice site falls below a few percent of the overall force on the composite. Our relaxation process leads to motions of the sites along the various coordinate axes. For simplicity, these motions are assumed to be mutually independent and we focus on displacements *along the y-axis* along which the composite is strained. Thus, the strain values ε (see Eq. (4)) are for elongations along the y-axis and they represent either an axial tensile strain (for bonds along the y-axis) or a shear strain (for bonds along the transverse x- and z-axes). Similarly, K in Eq. (4) denotes a tensile modulus (E_m or E_i) or a shear modulus (G_m or G_i).

Application of the model described above requires a detailed knowledge of the values for the activation energies U and activation volumes β (Eq. (3)) for the various types of bonds. These sets of values are rather difficult to determine experimentally. As in Ref. [16], we assume that both the inclusion and the matrix are isotropic so that U and β are the same for all the bonds belonging to the same component. Values of U and β for a given component (matrix or inclusion) are then selected so as to give reasonable values for its tenacity and elongation at break. Typical parameter values are as follows.

Testing conditions

The temperature is set equal to 23 °C and the rate of elongation equals 100% min^{-1}.

Inclusions

In Eqs. (3) and (4), we choose $U = 50$ kcal/mol, $\beta = (3.31\ \text{Å})^3$. Unless otherwise specified, we also take $E_i = 178$ GPa. (The latter value is equal to the tensile modulus of montmorillonite (MMT) platelets [4].) The above parameter values lead (at the selected testing conditions) to an elongation at break of around 6% and a tenacity of ~10 GPa. Poisson's ratio for the inclusion is set equal to 0.2 so that, $G_i = 74$ GPa.

Matrix

We take $U = 29$ kcal/mol, $\beta = (4.9\ \text{Å})^3$, and $E_m = 2.7$ GPa, equal to that of nylon-6 [4]. These values give an elongation and tenacity at break of 17% and 0.45 GPa, respectively. Taking Poisson's ratio equal to 0.35 leads to $G_m = 1$ GPa.

Interface

Unless otherwise specified, the interface between inclusions and matrix is given the same mechanical properties as those for the pure matrix.

3. Results and discussion

Fig. 2a–d shows model representations of several nanocomposite systems to be studied in this section. All the four figures are for a 1% volume fraction of inclusions with same aspect ratio $l/d = 40$ for ease of visualization. For platelets, l represents the diameter and d is the thickness, whereas for fibers, l is the length and d is the diameter. The tensile y-axis in Fig. 1 is along the vertical and the cube has side 200 nm.

Fig. 2a shows platelets randomly oriented with respect to the y-axis ($\langle \cos^2\theta \rangle = 0.33$, see Eq. (1) with $\lambda = 1$). Fig. 2b is the same but for fibers. Comparing with Fig. 2a, we note that fiber inclusions have a much higher surface area than platelets and hence the probability of fiber–fiber contacts is high even at a low V_i of 1%. In all our simulations of fiber-reinforced systems, the number of fiber–fiber contacts is minimized and our model predictions therefore represent ultimate properties. No such minimization has been attempted for the case of platelets because the incidence of platelet–platelet contacts is much lower. The case of platelets with high orientation, $\langle \cos^2\theta \rangle = 0.86$ is illustrated in Fig. 2c. Fig. 2d describes an intercalated system which was obtained by dispersing stacks of two platelets separated by a distance of 2 nm.

We now turn to a detailed study of the various factors controlling the tensile modulus of these nanostructures.

3.1. Effect of aspect ratio

Fig. 3 shows the effect of aspect ratio of the inclusion on composite modulus for the case of platelets (○) and fibers (●). The composite modulus predictions have been normalized by the matrix value, E_m. The figure is for $V_i = 3\%$ and perfect orientation of the inclusions along the tensile y-axis ($\langle \cos^2\theta \rangle = 1$). Both curves show the presence of two different regimes: a first regime in which modulus increases sharply with aspect ratio, followed by a second region in which the rise becomes slower. The transition between these two regimes is determined by the corresponding critical aspect ratio value which is required for these inclusions to reach the properties of infinitely large objects. For the case of fibers, the transition is observed at $l/d = 60$. The latter equals the critical aspect value obtained previously [21] for a single fiber with same E_i/E_m ratio. Because of their higher inertia, platelets have a higher critical aspect ratio than fibers, which explains the higher l/d value (~160 *vs.* 60 for fibers) at which the transition in Fig. 3 is observed. This is more clearly exemplified in Fig. 4 which shows strain profiles along the tensile y-axis within each type of inclusion for a value $l/d = 100$. The strain has been normalized by the overall strain on the composite. The figure clearly reveals that the fiber (●) easily reaches the overall composite strain in its middle section, thereby indicating that the critical aspect ratio value has been exceeded. In the case of platelets, on the other hand, the strain does not exceed 80% of the composite strain and the current aspect ratio $l/d = 100$ is less than critical. Further inspection of Fig. 3 also reveals that the platelets, although subcritical, provide a better reinforcement than fibers at all $l/d > 100$. These observations are in line with rotational isomeric state [8] and recent coarse-grained MD simulation [22] results. Also represented in Fig. 3 (----) are the predictions of the Halpin–Tsai equations which do not take into consideration the shape of the inclusions. Inspection of the figure reveals that these predictions

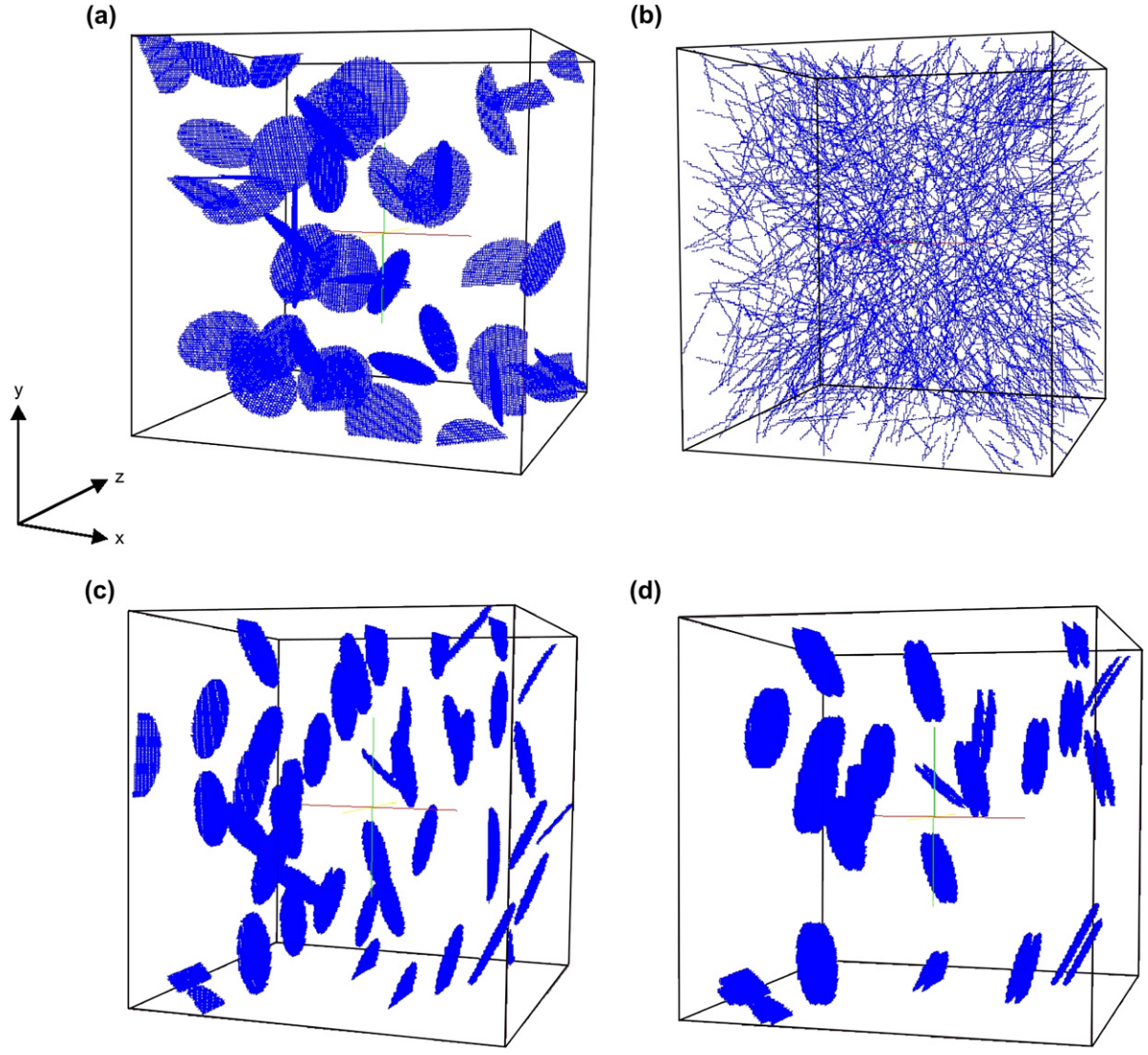

Fig. 2. Model representations of several nanocomposites with 1% inclusions of same aspect ratio 40: (a) randomly oriented platelets with $\cos^2\theta = 0.33$; (b) same but for fibers; (c) platelets oriented along the y-axis with $\cos^2\theta = 0.86$; (d) same as (c) but for an intercalated system made of stacks of 2 platelets at distance 2 nm. The tensile y-axis is along the vertical and the cube has side 200 nm.

follow our results for fibers and platelets at low and high aspect ratios, respectively.

3.2. Effect of orientation

The effect of the orientation factor $\cos^2\theta$ is studied in Fig. 5 at same $l/d = 100$ and $V_i = 3\%$. Both curves reveal a sharp increase in modulus at $\langle\cos^2\theta\rangle$ values larger than ~ 0.95, *i.e.* at angles $\theta < 13°$. The high anisotropy observed in Fig. 5 is due to the large mismatch in elastic modulus between the inclusion and the matrix. Our findings are very similar to those obtained for the development of modulus with orientation in crystalline fibers [23]. There, angles of less than 5°–10° between the polymer crystals and the fiber axis are required for achieving high stiffness in the fiber. Further inspection of Fig. 5 also reveals that platelets perform

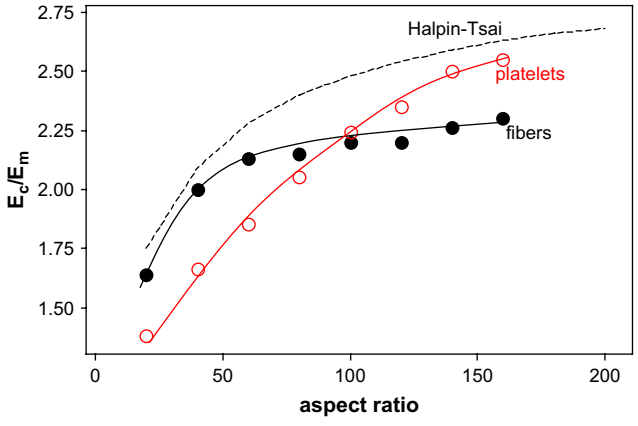

Fig. 3. Effect of aspect ratio l/d on composite modulus for platelets (○) and fibers (●) with $E_i = 178$ GPa. The composite modulus value has been normalized by E_m. The figure is for $V_i = 3\%$ and perfectly oriented inclusions $\langle\cos^2\theta\rangle = 1$. The curves are drawn to guide the eye.

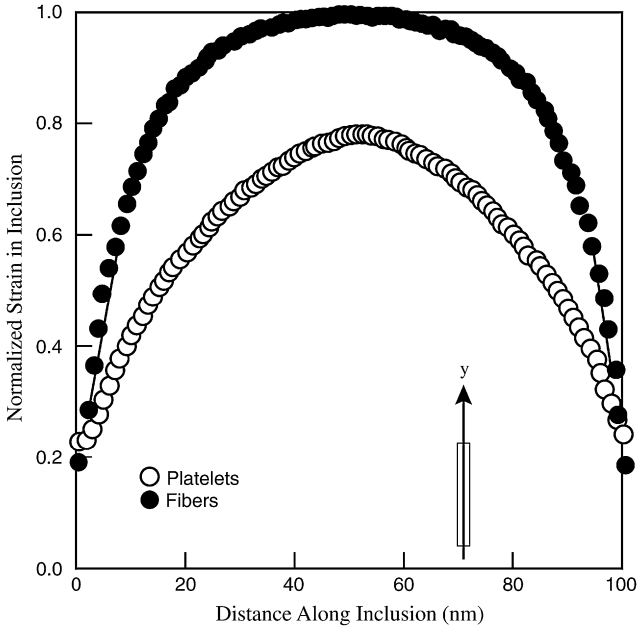

Fig. 4. Strain along the tensile y-axis within a fully oriented platelet (○) and fiber (●) with same aspect ratio $l/d = 100$.

significantly better than fibers at orientation levels $\langle \cos^2 \theta \rangle$ lower than 0.8, *i.e.* $\theta < 26°$.

3.3. Effect of the matrix/inclusion interface

An important feature of nanocomposites is the large contribution of the matrix/inclusion interface. Its effect is studied in Fig. 6 for increasing values of the interfacial modulus, $E_{m,i}$ (normalized by E_m). The figure is for fibers with $l/d = 100$,

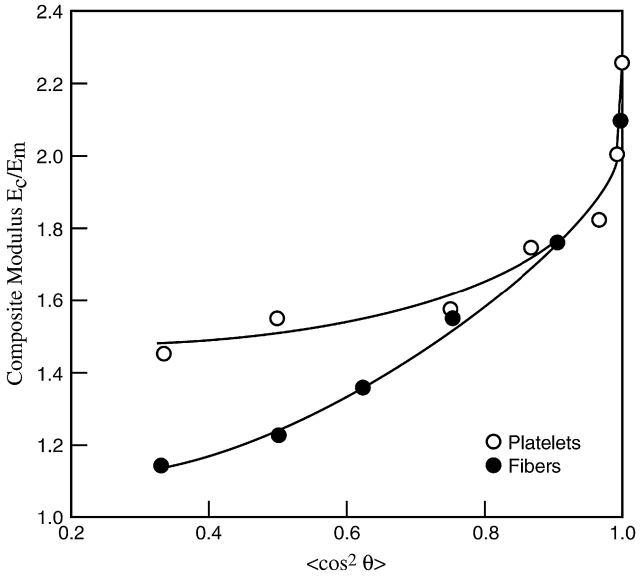

Fig. 5. Effect of inclusion orientation on composite modulus. The figure is for 3% inclusions with aspect ratio 100. The two sets of symbols are for platelets (○) and fibers (●). Both platelets and fibers have same $E_i = 178$ GPa and $G_i = 74$ GPa.

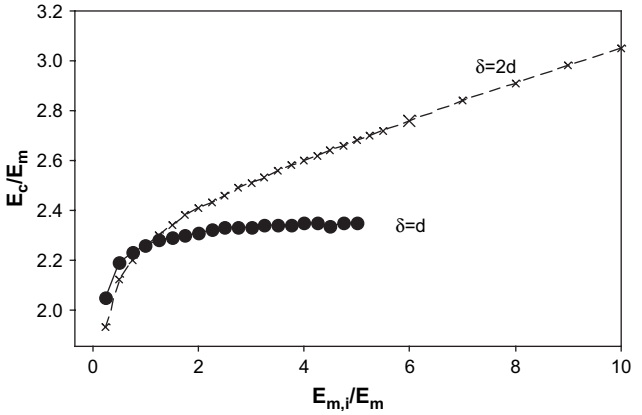

Fig. 6. Effect of interfacial modulus $E_{m,i}$ at two different values of the interface thickness δ. The figure is for fibers with $l/d = 100$, $V_i = 3\%$ and $\langle \cos^2 \theta \rangle = 1$.

$V_i = 3\%$, $\langle \cos^2 \theta \rangle = 1$ and two different values of the interface thickness δ (in units of the fiber diameter d). The results indicate that composite modulus increases with $E_{m,i}$ but quickly reaches a plateau value at small $\delta = d$. Turning to application to experiment, an increase in $E_{m,i}$ can be achieved through functionalization of the inclusion and subsequent crosslinking with the matrix (see for example, Ref. [24]). This process however is not expected to increase $E_{m,i}/E_m$ to values beyond the 2–3 range. Turning to our model predictions of Fig. 6, that increase in interface modulus leads to E_c/E_m values no higher than ~2.4, which is still below the 2.95 value obtained from the law of mixtures ($E_c/E_m = V_i \times E_i/E_m + (1 - V_i)$).

3.4. Effect of clustering of the inclusions

Fig. 7 shows our model predictions for platelets at increasing values of the number 'n' of platelets per cluster. These n-platelet clusters were dispersed in the matrix and given perfect orientation along the y-axis. The distance between platelets within a cluster is set equal to 2 nm, see also Fig. 2d. Our results reveal a linear decrease in modulus with the extent of clustering. These results are not surprising as an increase in the number of platelets per cluster is equivalent to a decrease in the effective aspect ratio of the reinforcement, see also Fig. 3.

3.5. Stress–strain curves and mode of failure

Fig. 8 shows our calculated stress–strain curves for the pure matrix (☒) and after reinforcement with 3% platelets (○) and fibers (●). Both types of inclusions have perfect orientation and aspect ratio equal to 100. Model results (not reproduced) reveal that, near 2.5% strain, the matrix starts to fail in tension near fiber ends or along the perimeter of the platelets. These interfacial cracks then propagate transversally deep inside the matrix and, in doing so, quickly become blunted by neighboring reinforcements. Upon further straining, the latter start to fail leading eventually to composite failure. Inspection of Fig. 8 reveals that platelets fail near 5%

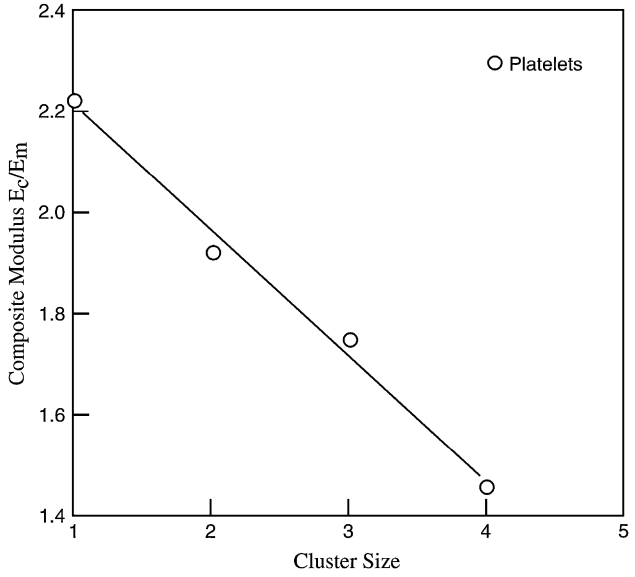

Fig. 7. Effect of clustering of the inclusions. The figure is for platelets with $l/d = 100$, $V_i = 3\%$ and $\langle \cos^2 \theta \rangle = 1$.

strain, versus a 6–7% value for fibers. As a result, fiber reinforcements lead to higher composite toughness, which compensates for their lower efficiency in increasing modulus.

3.6. Comparison to experiment for MMT platelets

Fig. 9 shows experimental data reported by Fornes and Paul [4] for montmorillonite (MMT) nanoplatelets (○) as well as for glass fibers (●) dispersed in nylon-6. The MMT platelets are reported to have exceptional exfoliation and their aspect ratio is estimated around $l/d = 100$ [4]. The platelets are also very well oriented along the tensile (flow) direction. The glass fibers, on the other hand, have $l/d = 20$ with a tensile modulus

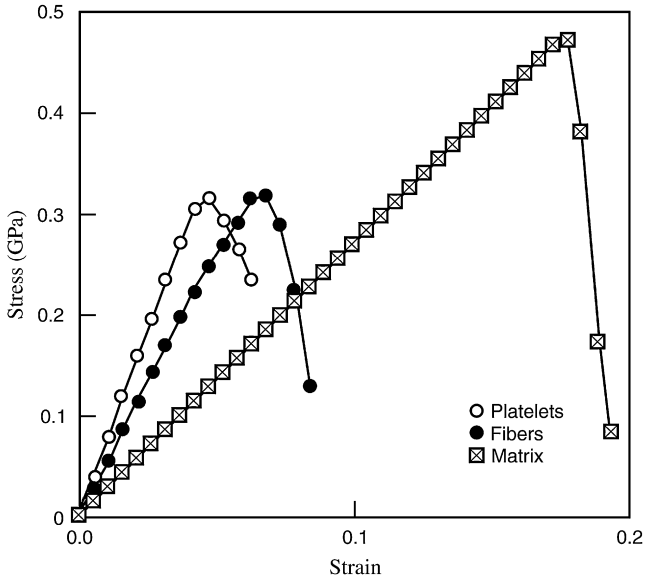

Fig. 8. Stress–strain curves for the matrix (⊠) and after reinforcement with 3% platelets (○) and fibers (●). Both types of inclusions have perfect orientation and aspect ratio equal to 100. The results are for an x–y–z lattice of $200 \times 200 \times 50$ lattice sites.

$E_f = 72$ GPa and Poisson's ratio equal to 0.2. At $V_i < 10\%$, the fiber orientation is reported to be poor, whereas at higher V_i, orientation greatly improves because of an increase in melt viscosity and filler–filler interactions [4]. Also reported in Fig. 9 are our model predictions for the two cases. The MMT platelets are for the case $l/d = 100$ and $\langle \cos^2 \theta \rangle = 1$. Model results for glass fibers are for $l/d = 20$ and two different orientation values: $\langle \cos^2 \theta \rangle = 1$ and $\langle \cos^2 \theta \rangle = 0.83$. Our predictions are in good agreement with experiment, which leads to confidence in the validity of our approach.

3.7. Application to carbon nanotubes (CNTs)

Recently, there has been a great interest in the use of carbon nanotubes (CNTs) for composite reinforcement [24]. That interest stems from their high aspect ratio and modulus value around 1000 GPa. Fig. 10 shows our model predictions for nanocomposites reinforced by platelets and fibers with $E_i = 1000$ GPa. The figure is for $V_i = 3\%$ and perfect orientation of the inclusions along the tensile y-axis ($\langle \cos^2 \theta \rangle = 1$). Our calculated curves follow the same trends as those obtained in Fig. 3 for softer inclusions ($E_i = 178$ GPa). The plateau values however are obtained at higher l/d values. For the case of fibers, a plateau is observed at $l/d = 120$ (*vs.* $l/d = 60$ in Fig. 3), which is again close to the critical aspect ratio value obtained previously [21] for $E_i = 1000$ GPa.

We now turn to comparison with experimental data of the tensile modulus of drawn fibers [25–27] reinforced with carbon nanotubes. The source of CNTs typically comes from Carbolex which consists of 2 μm ropes 10–20 nm in diameter with aspect ratio $l/d = 100$–200. Recent investigations of the ultrasonication techniques used to exfoliate these ropes into single nanotubes have revealed a substantial degradation in length [28]. Field-emission studies of exfoliated systems [29] indicate that the CNTs must be given an aspect ratio around 70 in order to obtain agreement with the Fowler–Nordheim equation. These observations are also in line with recent morphological studies [30]. In view of the above

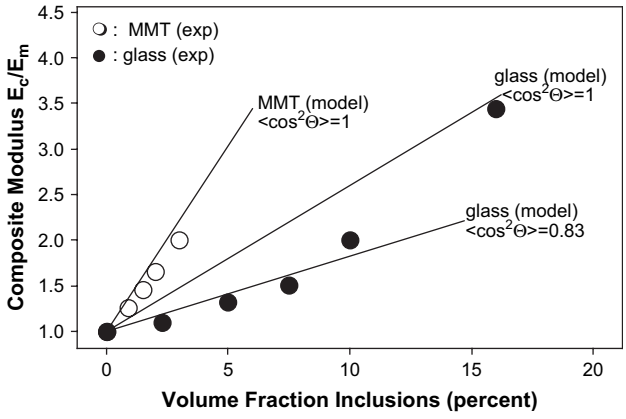

Fig. 9. Comparison with experimental data of Fornes and Paul [4] for MMT platelets (○) and short glass fibers (●). Our model results for MMT are for $l/d = 100$ and $\langle \cos^2 \theta \rangle = 1$. Model results for glass fibers are for $l/d = 20$ with $\langle \cos^2 \theta \rangle = 1$ and $\langle \cos^2 \theta \rangle = 0.83$. For glass, we took [4] $E_i = 72$ GPa and $G_i = 30$ GPa.

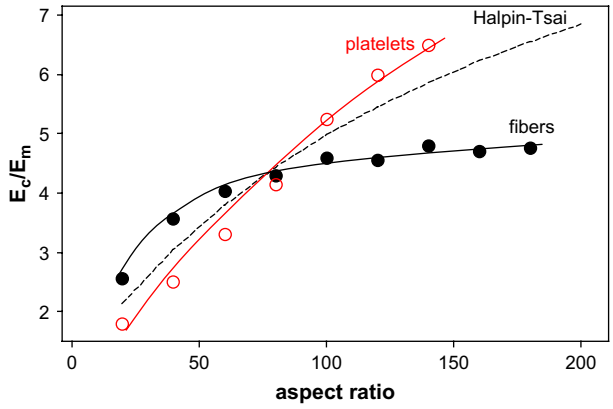

Fig. 10. Effect of aspect ratio l/d on composite modulus for inclusions with a modulus value $E_i = 1000$ GPa, typical of that for carbon nanotubes. The composite modulus value has been normalized by E_m. The figure is for $V_i = 3\%$ and perfectly oriented inclusions $\langle \cos^2 \theta \rangle = 1$. The curves are drawn to guide the eye.

consideration, we choose in our model simulations, a value $l/d = 70$. Since the results of Refs. [25–27] are for drawn fibers, we also take $\langle \cos^2 \theta \rangle = 1$. Comparison with experimental data is presented in Fig. 11. As in Fig. 9, model predictions are in good agreement with experiment.

4. Summary and conclusions

We have presented a numerical finite-difference model for the study of the factors controlling the properties of composites reinforced with platelets and fiber-like nano-particles. The approach is very flexible and it provides a comprehensive treatment of the dependence of composite modulus and strength on the shape of the inclusions and the interrelated effects of their orientation, volume fraction, aspect ratio, modulus and interfacial adhesion with the matrix.

At the same volume fraction, we find that platelets are generally more efficient than fibers in improving composite modulus. This is rationalized through our model finding that fibers have a typically low critical aspect ratio value, which puts an upper limit to their reinforcement potential. Platelets also turn out to be superior to fibers in all nanocomposites characterized by a poor orientation of the inclusions. We also find that low interfacial adhesion and poor dispersion of the inclusions lead to a decrease in reinforcement efficiency. Turning to comparison with experiment, a good agreement is found between our model predictions and modulus data on nanocomposites reinforced with montmorillonite platelets and carbon nanotubes.

It is important to stress that, being on a mesoscopic scale, our approach is incapable of predicting the properties of the interface between inclusion and matrix for a given system. Complicating effects such as filler-induced crystallization deep inside the matrix are also beyond the scope of this work [31].

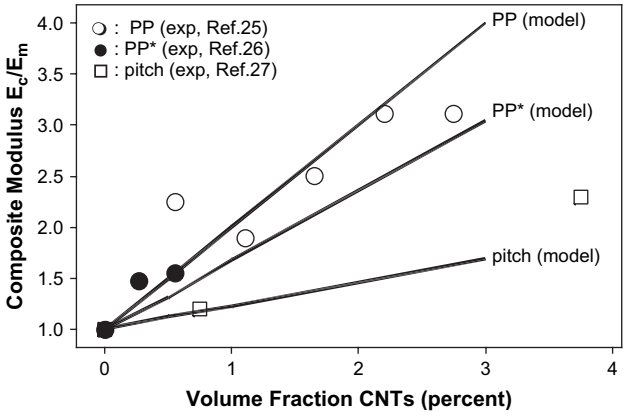

Fig. 11. Comparison with experimental data for carbon nanotubes (CNTs) in various fiber systems. Our model results are for $\langle \cos^2 \theta \rangle = 1$, $l/d = 70$ and $E_i = 1000$ GPa.

References

[1] Hui CY, Shia D. Polym Eng Sci 1998;38:774–82.
[2] Shia D, Hui CY, Burnside SD, Giannelis EP. Polym Compos 1998; 19:608–17.
[3] Brune DA, Bicerano J. Polymer 2002;43:369–87.
[4] Fornes TD, Paul DR. Polymer 2003;44:4993–5013.
[5] Luo J-J, Daniel IM. Compos Sci Technol 2003;63:1607–16.
[6] Odegard GM, Gates TS, Wise KE, Park C, Siochi EJ. Compos Sci Technol 2003;63:1671–87.
[7] Buxton GA, Balazs AC. J Chem Phys 2002;117:7649–59.
[8] Sharaf MA, Mark JE. Polymer 2002;43:643–52.
[9] Smith JS, Bedrov D, Smith GD. Compos Sci Technol 2003;63: 1599–605.
[10] Frankland SJV, Harik VM, Odegard GM, Brenner DW, Gates TS. Compos Sci Technol 2003;63:1655–61.
[11] Hine PG, Lusti HR, Gusev AA. Compos Sci Technol 2002;62:1445–53.
[12] Fisher FT, Bradshaw RD, Brinson LC. Compos Sci Technol 2003;63:1689–703.
[13] Miyagawa H, Rich MJ, Drzal LT. J Polym Sci Part B Polym Phys 2004;42:4391–400.
[14] Termonia Y. J Mater Sci 1990;25:4644–9.
[15] Termonia Y. J Mater Sci 1992;27:4878–82.
[16] Termonia Y. J Polym Sci Part B Polym Phys 1994;32:969–79.
[17] Kausch HH. Polymer fracture. Berlin: Springer-Verlag; 1987.
[18] Zhang D, Meyer H. J Polym Sci Part B Polym Phys 2007;45:2161–6.
[19] Kuhn W, Grun F. Kolloid-Z 1942;101:248.
[20] Termonia Y, Smith P. Polymer 1986;27:1845–9.
[21] Termonia Y. J Mater Sci Lett 1993;12:732–3.
[22] Knauert ST, Douglas JF, Starr FW. J Polym Sci Part B Polym Phys 2007;45:1882–97.
[23] Bastiaansen CWM, Leblans PJR, Smith P. Macromolecules 1990;23: 2365–70.
[24] Moniruzzaman M, Winey KI. Macromolecules 2006;39:5194–205.
[25] Kearns JC, Shambaugh RL. J Appl Polym Sci 2002;86:2079–84.
[26] Chang TE, Jensen LR, Kisliuk A, Pipes RB, Pyrz R, Sokolov AP. Polymer 2005;46:439–44.
[27] Andrews R, Jacques D, Rao AM, Rantell T, Derbyshire F. Appl Phys Lett 1999;75:1329–32.
[28] Cotiuga I, Picchioni F, Agarwal US, Wouters D, Looj J, Lemstra PJ. Macromol Rapid Commun 2006;27:1073–8.
[29] Alexandrou I, Kymakis E, Amaratunga GAJ. Appl Phys Lett 2002;80:1435–8.
[30] Loos J, Grossiord N, Koning CE, Regev O. Compos Sci Technol 2007;67:783–8.
[31] Ryan KP, Cadek M, Nicolosi V, Blond D, Ruether M, Armstrong G, et al. Compos Sci Technol 2007;67:1640–9.